Bibliographical reference

Wave Based Modeling of the Sound Insulation of Double Walls With Structural Connections, A. Dijckmans, Acta Acustica **vol. 103** (Number 3), 2017, pp. 465-479

DOI
https://doi.org/10.3813/AAA.919076

Acta Acustica united with Acustica
Vol. 103 (2017) 465 – 479

DOI 10.3813/AAA.919076

Wave Based Modeling of the Sound Insulation of Double Walls With Structural Connections

A. Dijckmans*
KU Leuven, Department of Civil Engineering, Kasteelpark Arenberg 40, 3001 Leuven, Belgium.
arne.dijckmans@bbri.be

Summary
In this paper, a wave based model is developed for the investigation of the direct sound transmission through double walls with structural connections placed between two rooms. The modal behaviour of the rooms and the structure is taken into account. Point and line connections with an increasing degree of complexity are introduced in the double wall model to incorporate the effect of structure-borne paths. The studs and ties are modeled as rigid connections or a combination of translational and rotational springs. Alternatively, the studs are modeled as beams, accounting for the modal behaviour of the studs. The wave based results are compared with experiments and infinite plate models based on a decoupled approach or a periodic approach. It is shown that the finite dimensions can have a significant influence on the sound insulation, both at low frequencies and at higher frequencies. The pass- and stop-band behaviour predicted for periodic structures cannot fully develop in finite double walls. Furthermore, the stud spacing can influence the resonant behaviour of the TL at low and mid frequencies, but has limited effect at higher frequencies.

PACS no. 4355.Ka, 43.55.Rg, 43.55.Ti

1. Introduction

Double walls are widely used in buildings as internal partitions or as party walls between apartments. This type of walls can provide good sound insulation with a relatively low weight. The acoustic performance of double leaf walls is often determined by structure-borne sound transmission through mechanical links between the two leaves, like studs or ties. The transmission loss (TL) of double panels with structural links has been studied extensively in literature, both experimentally and theoretically.

Hongisto *et al.* [1] carried out a comprehensive experimental parametric study of steel double walls, including both uncoupled walls and walls coupled by steel or wooden studs. For the double walls with studs, the stiffness or type of the stud and the spacing of the screws between the panel and the stud were the most influencing parameters. The stud spacing did have less influence on the TL than expected, especially at high frequencies, although it did strongly influence the resonance dips at lower frequencies for the double panels with wooden studs.

Structural coupling can be simply introduced in statistical energy analysis (SEA) models as a coupling loss factor between the plates [2]. Craik and Wilson [3] developed expressions for the case of point connections and applied the models to masonry cavity walls with metal ties. Craik and Smith [4] elaborated expressions for coupling loss factors for line connections using either beam or plate theory for the stud. SEA predictions were compared with measurements of plasterboard walls screwed to a wooden frame. A transition from line to point coupling behaviour was found when half a bending wavelength fits between two screws on the plate.

Semi-analytical prediction models [5, 6, 7, 8, 9] address the sound transmission through double walls with structural links by decoupling the total transmission in terms of an airborne path through the cavity and a structure-borne path through the structural links, under the assumption of infinite plates and diffuse incident sound fields. Sharp [5] developed semi-analytical formulas for rigid and massless point or line connections. Fahy and Gardonio [6] extended the models to incorporate the mass of the studs. Davy [7] included the compliance of the studs and modeled the line connections as mass-spring-mass systems. He accounted for the resonant response of the panels so that the semi-analytical model can also be used around and above the critical frequency of the panels. Vigran [8] incorporated the theory of Sharp for massless and rigid connections in a transfer matrix setup. Reasonable agreement was found with TL measurements of lightweight constructions with wooden studs and a heavy wall. In [9], the transfer matrix model was further extended to include flexible studs. These semi-analytical models all use a smeared representation of the structural connections, i.e. the connections are assumed to be distributed uniformly between the panels. In

Received 30 September 2016,
accepted 2 April 2017.

* Present address: Belgian Building Research Institute, Lombardstraat 42, 1000 Brussels, Belgium

this way, the discrete placing of the point and line connections is disregarded and periodic effects are not accounted for.

A second type of analytical models assume infinite structures with periodically placed studs [10, 11, 12, 13, 14, 15, 16]. The periodicity of the structure allows the use of Fourier transform techniques to solve the problem in the wavenumber domain. Lin and Garrelick [10] investigated the TL of double walls with rigid, massless studs. Brunskog and Hammer [11] applied the Fourier transform technique for the prediction of the impact sound level of lightweight floors with rigid studs. The model was improved by Mosharrof *et al.* [12] by including beam elements and the effect of moment reactions between beams and plates. Wang *et al.* [13] showed the influence of the pass- and stop-bands of periodic structures by comparing a periodic model with a smeared model. The studs were modeled as translational and rotational springs. Legault and Atalla [14] investigated the TL of a double aluminum panel by means of periodic plate models with an increasing amount of complexity. The studs were either modeled as rigid and massless, as mass-spring-mass connections or as beam elements. The models were also compared with the decoupled approaches of Sharp [5], Fahy [6] and Davy [7]. They further investigated the effect of resilient mounts between the panel and the studs in [15]. Xin and Lu [16] extended the Fourier transform technique to double panels with periodically placed studs in two orthogonal directions.

The assumptions made in the analytical and statistical models, like high modal density and modal overlap, are often not satisfied in laboratory and real conditions. Previously, the author has developed a wave based model to predict the airborne sound transmission through double walls between two rooms, taking into account the modal behaviour of the rooms and the structure [17]. It was shown that the modal behaviour of the double wall can play an important role in a broad frequency range. In this paper, the sound transmission through finite double walls with structural point or line connections is investigated. Relatively few studies treating this problem have been reported in literature. Díaz-Cereceda *et al.* [18] used modal analysis to predict the vibration level difference between coupled plates in the case of mechanical excitation. They for example investigated the influence of the position of the studs, showing that a stud at the border of a plate leads to a larger vibration transmission than a stud in the middle. Arjunan *et al.* [19] developed a finite element model for the airborne sound transmission through gypsum plasterboard walls with steel studs. Due to the high computational cost, calculations were only performed at three frequencies per 1/3 octave band. The computational efficiency of the wave based model allows a more detailed analysis of the TL over frequency, which is important when the fluctuations due to the modal behaviour are large.

Most studies described above use simplified theoretical models for the structural connections. Typically, ideal point or line connections are assumed. Often, the connections are assumed rigid [5, 8, 10, 11] or modeled as translational and/or rotational springs [7, 9, 13]. The stiffness of the springs can be frequency dependent [9, 20, 21]. More refined models have also been used for the studs in double walls, applying beam theory [12, 16], plate theory [4] or full 3D models [19]. Galbrun [22] examined the applicability and limitations of these fundamental theories by comparing measurements and simulations for point-connected lightweight structures consisting of timber beams and plasterboard plates. Simple point models proved only valid at low and mid frequencies, and it was shown that both force and moment transmission across studs should be accounted for.

In this paper, a deterministic wave based model (WBM) is developed to assess the direct sound transmission through double walls with structural connections placed between two rooms. Point and line connections with an increasing amount of complexity are introduced in the original model for double walls [17]. The model, which is described in detail in section 2, is used to investigate the sound transmission through several types of double walls with structural connections. The test panels used in the study are described in section 3. The WBM results are compared with semi-analytical and periodic infinite plate model results in section 4. A parametric study further shows the influence of stud properties, stud spacing, edge connections, and room dimensions on the TL. The models are validated with experimental results in section 5. Conclusions are given in section 6.

2. Wave based model

2.1. Problem definition

Figure 1 gives a schematic overview of the model. A rectangular double wall with dimensions $L_{\mathrm{p}x}$ and $L_{\mathrm{p}y}$ is placed between two 3D rectangular rooms with rigid side and back walls. Source and receiving room have dimensions $L_x^{(1)} \times L_y^{(1)} \times L_z^{(1)}$ and $L_x^{(3)} \times L_y^{(3)} \times L_z^{(3)}$, respectively. The side walls of the cavity with dimensions $L_x^{(2)} \times L_y^{(2)} \times L_z^{(2)}$ are also assumed rigid. A harmonic volume point source is placed in the source room at position $(x_\mathrm{s}, y_\mathrm{s}, z_\mathrm{s})$. Flanking transmission is neglected. The plates have simply supported boundary conditions and are assumed homogeneous, isotropic and acoustically thin. The two plates are connected by N_s point connections and N_l vertical line connections. It is assumed that the vertical line connections extend over the entire height of the w all, i.e. that they have a length of $L_{\mathrm{p}y}$. Horizontal line connections are not considered in this section but can be taken into account in a similar way. The point and line connections are modeled as massless rigid or massless spring connections. Alternatively, a beam model is used for the line connections.

2.1.1. Rooms and air cavity

The source room is divided into two subdomains ($V^{(0)}$ and $V^{(1)}$) by a plane through the point source, parallel to the back wall. It is assumed that the structural connections in

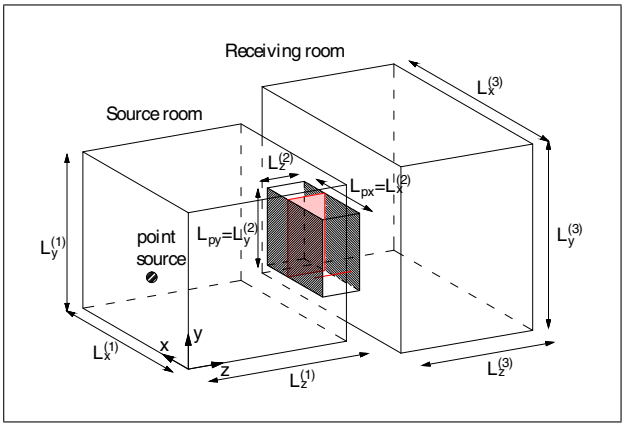

Figure 1. Geometry of the wave based model: a double wall with structural point and line connections, placed between two rooms with rigid side and back walls.

the cavity ($V^{(2)}$) of the double wall are acoustically transparent, i.e. that they do not block the acoustic waves in the cavity. Brunskog [23] showed that this assumption is valid when structure–borne transmission dominates over the airborne path. When cavity absorption is present, the effect of the partitioning on the sound field in the cavity will even be smaller [15]. The steady-state acoustical pressure $\underline{p}_{\mathrm{a}}^{(i)}$ in each (sub)room $V^{(i)}$ ($i = 0 \ldots 3$) is governed by the homogeneous Helmholtz equation,

$$\nabla^2 \underline{p}_{\mathrm{a}}^{(i)} + k_{\mathrm{a}}^2 \underline{p}_{\mathrm{a}}^{(i)} = 0. \tag{1}$$

$k_{\mathrm{a}} = \frac{\omega}{c_{\mathrm{a}}}$ is the acoustic wave number in air, with ω the circular frequency and c_{a} the speed of sound in air. The underscore (_) denotes a complex value throughout the paper. In source and receiving room, uniform spatial damping is introduced by making the acoustic wave number complex,

$$\underline{k}_{\mathrm{a}}^{(i)} = k_{\mathrm{a}} \left(1 - \mathrm{j}\frac{1}{2}\frac{2.2}{f T^{(i)}}\right), \tag{2}$$

where $T^{(i)}$ is the reverberation time of the room. f is the frequency, $\mathrm{j} = \sqrt{-1}$.

2.1.2. Rigid and spring connections

Each point connection ($i = 1 \ldots N_{\mathrm{s}}$) is modeled as a massless translational spring with a stiffness $K_{\mathrm{t}i}$. The stiffness links the force $\underline{F}_{\mathrm{s}i}$ in the spring to the transverse displacement of the two panels at the connection,

$$\underline{w}_{\mathrm{p}}^{(1)}(x_{\mathrm{s}i}, y_{\mathrm{s}i}) - \underline{w}_{\mathrm{p}}^{(2)}(x_{\mathrm{s}i}, y_{\mathrm{s}i}) = \frac{\underline{F}_{\mathrm{s}i}}{K_{\mathrm{t}i}}, \tag{3}$$

with $(x_{\mathrm{s}i}, y_{\mathrm{s}i})$ the position of point connection i. $\underline{w}_{\mathrm{p}}^{(1)}$ is the transverse displacement of the first panel at the source side and $\underline{w}_{\mathrm{p}}^{(2)}$ is the transverse displacement of the second panel at the receiving side.

Each line connection ($i = 1 \ldots N_{\mathrm{l}}$) is modeled as a combination of a massless translational spring with stiffness per unit length $K'_{\mathrm{t}i}$ and a massless rotational spring with stiffness per unit length $K'_{\mathrm{r}i}$. The force $\underline{F}'_{\mathrm{l}i}$ and moment $\underline{M}'_{\mathrm{l}i}$ per unit length for each line connection i are linked to the displacement and rotation of the two panels at the line connection by

$$\underline{w}_{\mathrm{p}}^{(1)}(x_{\mathrm{l}i}, y) - \underline{w}_{\mathrm{p}}^{(2)}(x_{\mathrm{l}i}, y) = \frac{\underline{F}'_{\mathrm{l}i}(y)}{K'_{\mathrm{t}i}}, \tag{4}$$

$$\frac{\partial \underline{w}_{\mathrm{p}}^{(1)}(x_{\mathrm{l}i}, y)}{\partial x} - \frac{\partial \underline{w}_{\mathrm{p}}^{(2)}(x_{\mathrm{l}i}, y)}{\partial x} = \frac{\underline{M}'_{\mathrm{l}i}(y)}{K'_{\mathrm{r}i}}, \tag{5}$$

with $x_{\mathrm{l}i}$ the position of the vertical line connection i.

Rigid point and line connections can be incorporated in a straightforward way by setting the compliances $C_{\mathrm{t}i} = 1/K_{\mathrm{t}i}$, $C'_{\mathrm{t}i} = 1/K'_{\mathrm{t}i}$ and $C'_{\mathrm{r}i} = 1/K'_{\mathrm{r}i}$ equal to zero.

2.1.3. Beams

For beams with a symmetric cross-section, the translational displacement $\underline{w}_{\mathrm{bz}i}$ and rotational displacement $\underline{\theta}_{\mathrm{by}i}$ of each beam ($i = 1 \ldots N_{\mathrm{l}}$) are governed by following uncoupled equations:

$$\left[\underline{B}_{\mathrm{b}i}\frac{\partial^4}{\partial y^4} - \omega^2 m'_{\mathrm{b}i}\right] \underline{w}_{\mathrm{bz}i} = \underline{F}'^{(1)}_{\mathrm{l}i} - \underline{F}'^{(2)}_{\mathrm{l}i}, \tag{6}$$

$$\left[\underline{W}_{\mathrm{b}i}\frac{\partial^4}{\partial y^4} + \underline{T}_{\mathrm{b}i}\frac{\partial^2}{\partial y^2} - \omega^2 I'_{\mathrm{bS}i}\right] \underline{\theta}_{\mathrm{by}i} = \underline{M}'^{(1)}_{\mathrm{l}i} - \underline{M}'^{(2)}_{\mathrm{l}i}. \tag{7}$$

$\underline{F}'^{(1)}_{\mathrm{l}i}$ and $\underline{M}'^{(1)}_{\mathrm{l}i}$ are the force and moment per unit length exerted by plate 1 on the beam. $\underline{F}'^{(2)}_{\mathrm{l}i}$ and $\underline{M}'^{(2)}_{\mathrm{l}i}$ are the force and moment exerted by plate 2. The beam bending stiffness $\underline{B}_{\mathrm{b}i}$, torsional stiffness $\underline{T}_{\mathrm{b}i}$ and warping stiffness $\underline{W}_{\mathrm{b}i}$ are defined as

$$\underline{B}_{\mathrm{b}i} = E_{\mathrm{b}i}(1 + j\eta_{\mathrm{b}i})I_{xi}, \tag{8}$$

$$\underline{T}_{\mathrm{b}i} = G_{\mathrm{b}i}(1 + j\eta_{\mathrm{b}i})J_{yi}, \tag{9}$$

$$\underline{W}_{\mathrm{b}i} = E_{\mathrm{b}i}(1 + j\eta_{\mathrm{b}i})I_{wi}, \tag{10}$$

with I_{xi} the second moment of area with respect to the x-axis, J_{yi} the torsional constant in the y-direction and I_{wi} the warping constant. $m'_{\mathrm{b}i}$ is the mass per unit length and $I'_{\mathrm{bS}i}$ the moment of inertia per unit length of beam i. The material of beam i has a Young's modulus $E_{\mathrm{b}i}$, a shear modulus $G_{\mathrm{b}i}$ and a loss factor $\eta_{\mathrm{b}i}$.

2.1.4. Plates

The transverse displacements $\underline{w}_{\mathrm{p}}^{(j)}$ of the plates ($j = 1, 2$) fulfil Kirchhoff's thin plate bending wave equation,

$$\begin{aligned}\left[\underline{B}'_1 \nabla^4 - \omega^2 m''_1\right] \underline{w}_{\mathrm{p}}^{(1)} = \\ \underline{p}_{\mathrm{a}}^{(1)} - \underline{p}_{\mathrm{a}}^{(2)} - \sum_{i=1}^{N_{\mathrm{s}}} \left[\underline{F}_{\mathrm{s}i}\delta(x - x_{\mathrm{s}i}, y - y_{\mathrm{s}i})\right] \\ - \sum_{i=1}^{N_{\mathrm{l}}} \left[\underline{F}'^{(1)}_{\mathrm{l}i}\delta(x - x_{\mathrm{l}i}) - \frac{\partial}{\partial x}\underline{M}'^{(1)}_{\mathrm{l}i}\delta(x - x_{\mathrm{l}i})\right],\end{aligned} \tag{11}$$

$$\left[\underline{B}_2'\nabla^4 - \omega^2 m_2''\right]\underline{w}_{\mathrm{p}}^{(2)} = \underline{p}_{\mathrm{a}}^{(2)} - \underline{p}_{\mathrm{a}}^{(3)} + \sum_{i=1}^{N_{\mathrm{s}}}\left[\underline{F}_{si}\delta(x-x_{si}, y-y_{si})\right] + \sum_{i=1}^{N_{\mathrm{l}}}\left[\underline{F}_{\mathrm{l}i}'^{(2)}\delta(x-x_{\mathrm{l}i}) - \frac{\partial}{\partial x}\underline{M}_{\mathrm{l}i}'^{(2)}\delta(x-x_{\mathrm{l}i})\right], \tag{12}$$

where the plate bending stiffness $\underline{B}_j'$ is defined as

$$\underline{B}_j' = \frac{E_j h_j^3(1+j\eta_j)}{12(1-\nu_j^2)}. \tag{13}$$

$m_j'' = \rho_j h_j$ is the surface mass density and h_j the thickness of plate j. The material of plate j has a density ρ_j, a Young's modulus E_j, a loss factor η_j and a Poisson's ratio ν_j. δ is the Dirac delta function. The equations of motion account for the fluid loading and the forces and moments exerted by the point and line connections. In the case of rigid or spring connections, the forces and moments exerted on plate 1 and plate 2 are the same: $\underline{F}_{\mathrm{l}i}'^{(1)} = \underline{F}_{\mathrm{l}i}'^{(2)} = \underline{F}_{\mathrm{l}i}'$ and $\underline{M}_{\mathrm{l}i}'^{(1)} = \underline{M}_{\mathrm{l}i}'^{(2)} = \underline{M}_{\mathrm{l}i}'$.

2.2. Field variable expansions

The acoustic pressures are approximated in terms of the following acoustic wave function expansion:

$$\underline{\hat{p}}_{\mathrm{a}}^{(i)} = \sum_{m,n}\left[\mathrm{e}^{-\mathrm{j}\underline{k}_{z,mn}^{(i)}z}\underline{P}_{mn}^{(i)} + \mathrm{e}^{\mathrm{j}\underline{k}_{z,mn}^{(i)}z}\underline{Q}_{mn}^{(i)}\right] \cdot\cos\left(\frac{m\pi}{L_x^{(i)}}x\right)\cos\left(\frac{n\pi}{L_y^{(i)}}y\right), \tag{14}$$

where

$$\underline{k}_{z,mn}^{(i)} = \sqrt{\left(\underline{k}_{\mathrm{a}}^{(i)}\right)^2 - \left(\frac{m\pi}{L_x^{(i)}}\right)^2 - \left(\frac{n\pi}{L_y^{(i)}}\right)^2}, \tag{15}$$

with m, n = 0,1,2,.... The wave functions are exact solutions of the homogeneous Helmholtz equation. The time dependence $\mathrm{e}^{\mathrm{j}\omega t}$ has been omitted throughout the paper.

Using Euler's equation, equation (14) leads to following wave function expansion for the air particle displacement in the z-direction,

$$\underline{\hat{w}}_{\mathrm{a}}^{(i)} = \frac{-\mathrm{j}}{\omega^2\rho_{\mathrm{a}}}\sum_{m,n}\left[\mathrm{e}^{-j\underline{k}_{z,mn}^{(i)}z}\underline{P}_{mn}^{(i)} - \mathrm{e}^{\mathrm{j}\underline{k}_{z,mn}^{(i)}z}\underline{Q}_{mn}^{(i)}\right] \cdot\underline{k}_{z,mn}^{(i)}\cos\left(\frac{m\pi}{L_x^{(i)}}x\right)\cos\left(\frac{n\pi}{L_y^{(i)}}y\right), \tag{16}$$

with ρ_{a} the density of air.

The transverse displacement of the acoustically thin plates ($j = 1, 2$) is written as an expansion series,

$$\underline{\hat{w}}_{\mathrm{p}}^{(j)} = \sum_{p,q}\underline{A}_{pq}^{(j)}\sin\left(\frac{p\pi}{L_{\mathrm{p}x}}x\right)\sin\left(\frac{q\pi}{L_{\mathrm{p}y}}y\right), \tag{17}$$

with p, q = 1,2,3,.... These expansion functions satisfy a priori the simply supported boundary conditions.

The forces and moments in each line connection ($i = 1 \ldots N_{\mathrm{l}}$, $j = 1, 2$) are also written as an expansion series,

$$\underline{\hat{F}}_{\mathrm{l}i}'^{(j)} = \sum_q \underline{F}_{\mathrm{l}i,q}'^{(j)}\sin\left(\frac{q\pi}{L_{\mathrm{p}y}}y\right), \tag{18}$$

$$\underline{\hat{M}}_{\mathrm{l}i}'^{(j)} = \sum_q \underline{M}_{\mathrm{l}i,q}'^{(j)}\sin\left(\frac{q\pi}{L_{\mathrm{p}y}}y\right). \tag{19}$$

The beam displacements ($i = 1 \ldots N_{\mathrm{l}}$) are expanded as

$$\underline{\hat{w}}_{\mathrm{b}zi} = \sum_q \underline{w}_{\mathrm{b}zi,q}\sin\left(\frac{q\pi}{L_{\mathrm{p}y}}y\right), \tag{20}$$

$$\underline{\hat{\theta}}_{\mathrm{b}yi} = \sum_q \underline{\theta}_{\mathrm{b}yi,q}\sin\left(\frac{q\pi}{L_{\mathrm{p}y}}y\right). \tag{21}$$

2.3. Boundary and continuity conditions

For ease of notation, the boundary and continuity conditions are written in a local coordinate system, where the origin of the local coordinate systems is placed at the bottom left corner of each room.

At the rigid back walls of source and receiving room, the air particle displacement must be zero,

$$\underline{\hat{w}}_{\mathrm{a}}^{(0)}(x, y, 0) = 0, \tag{22}$$

$$\underline{\hat{w}}_{\mathrm{a}}^{(3)}(x, y, L_z^{(3)}) = 0. \tag{23}$$

At the plates surfaces, continuity of transverse displacement is imposed,

$$\underline{\hat{w}}_{\mathrm{a}}^{(1)}(x, y, L_z^{(1)}) = \underline{\hat{w}}_{\mathrm{p}}^{(1)}(x, y) = \underline{\hat{w}}_{\mathrm{a}}^{(2)}(x, y, 0), \tag{24}$$

$$\underline{\hat{w}}_{\mathrm{a}}^{(2)}(x, y, L_z^{(2)}) = \underline{\hat{w}}_{\mathrm{p}}^{(2)}(x, y) = \underline{\hat{w}}_{\mathrm{a}}^{(3)}(x, y, 0). \tag{25}$$

For the case of beams coupling the two plates, continuity of transverse displacement and rotation is imposed,

$$\underline{\hat{w}}_{\mathrm{p}}^{(1)}(x_{\mathrm{l}i}, y) = \underline{\hat{w}}_{\mathrm{b}zi}(y) = \underline{\hat{w}}_{\mathrm{p}}^{(2)}(x_{\mathrm{l}i}, y), \tag{26}$$

$$\frac{\partial\underline{\hat{w}}_{\mathrm{p}}^{(1)}(x_{\mathrm{l}i}, y)}{\partial x} = \underline{\hat{\theta}}_{\mathrm{b}yi}(y) = \frac{\partial\underline{\hat{w}}_{\mathrm{p}}^{(2)}(x_{\mathrm{l}i}, y)}{\partial x}. \tag{27}$$

2.4. Construction of system matrices and post-processing

Because the proposed pressure expansions are exact solutions of the homogeneous Helmholtz equation, the participation factors $\underline{P}_{mn}^{(i)}$ and $\underline{Q}_{mn}^{(i)}$ are only determined by the boundary and continuity conditions. The pressure expansion functions satisfy a priori the rigid wall boundary conditions. The other boundary and continuity conditions can only be satisfied approximately, as only a finite number of expansion functions can be taken into account. The chosen number of wave functions is based on a truncation criterium such that all wave functions with a wavenumber smaller than two times the maximum natural wavenumber in the system are taken into account [17]. The residuals on the boundaries are minimized in an integral sense using a Galerkin weighted residual formulation [17]. The sine and

cosine wave functions used in the field variable expansions are used as weighting functions. Because of the rectangular geometry, the factors $\underline{P}_{mn}^{(i)}$ and $\underline{Q}_{mn}^{(i)}$ can be eliminated analytically in function of the unknowns $\underline{A}_{pq}^{(j)}$ by use of the weighted residual formulation of the boundary and continuity conditions (22)-(25). Equations (12) and (13) for the plates, equations (6) and (7) for the beams, and equations (3)-(5) for the spring connections are also solved by means of a weighted residual formulation. This results in a symmetric set of linear equations in the primary unknowns $\underline{A}_{pq}^{(j)}$, $\underline{F}_{\mathrm{s}i}$, $\underline{F}_{\mathrm{l}i,q}^{\prime(j)}$, $\underline{M}_{\mathrm{l}i,q}^{\prime(j)}$, $\underline{w}_{\mathrm{b}zi,q}$ and $\underline{\theta}_{\mathrm{b}yi,q}$.

The additional computational effort to include structural connections in the wave based model is limited, because the structural connections do not influence the original matrix elements for the double wall model without structural connections. It only results in additional columns and rows.

After the wave function contribution factors are determined, the TL is determined by following measurement formula:

$$\mathrm{TL} = L_{p\mathrm{e}} - L_{p\mathrm{r}} + 10\lg\left(S/A_{\mathrm{r}}\right), \tag{28}$$

where $L_{p\mathrm{e}}$ and $L_{p\mathrm{r}}$ are the average sound pressure level in emitting and receiving room, S ($= L_{\mathrm{p}x}L_{\mathrm{p}y}$) is the surface area of the wall and $A_{\mathrm{r}} = \frac{0.16V_{\mathrm{r}}}{T_{\mathrm{r}}}$ the absorption area of the receiving room, with V_{r} ($= L_x^{(3)}L_y^{(3)}L_z^{(3)}$) the volume and T_{r} the reverberation time. Calculations are performed at 81 frequencies per one-third octave band and averaged in 1/12 or 1/3 octave bands.

It can be noted here that it is not the aim of the paper to follow the specifications of the standard ISO 10140 [24, 25] when determining the TL with the WBM. The average sound pressure levels in the rooms are determined analytically over the entire volume of the rooms, thus avoiding uncertainties related to the spatial sampling of the sound field in measurements. Furthermore, only one source position has been used in the WBM in this paper, unless stated otherwise. While the WBM results are thus not entirely representative for standardized laboratory measurements, it can give good insight in the effects of geometrical parameters like room and plate dimensions on the TL. The influence of several parameters related to the measurement set-up on the repeatability and reproducibility has been thoroughly discussed in [26] and [27]. Variations related to the source and microphone positions are mainly important below the Schroeder frequency of the rooms and the reproducibility uncertainty is generally much larger than the repeatability uncertainty.

3. Test panels

Four types of double walls are considered in this paper: a double aluminum panel, a wooden floor, double gypsum fiberboard walls with a steel stud frame, and a double gypsum fiberboard wall with a timber stud frame. The aluminum panel has been extensively investigated in [14]. The wooden floor is based on the structure investigated in [11]. The double gypsum fiberboard walls with steel studs were part of a measurement campaign carried out previously at the Laboratory of Acoustics of KU Leuven. The double wall with a timber stud frame has been used in an experimental investigation in [28]. The TL of the structures is simulated with the WBM and two different infinite plate models: the decoupled model of Davy [7] and the infinite periodic plate model of Legault and Atalla [14].

Table I. Material properties of the test panels used in the simulations.

	ρ [kg/m^3]	E [MPa]	η [-]	ν [-]
Aluminum	2742	70000	0.01	0.33
Wood (plate)	500	6550	0.01	0.30
Wood (stud)	500	9800	0.015	0.30
Gypsum (steel stud)	720	2500	0.03	0.30
Gypsum (timber stud)	1225	4400	0.03	0.30

3.1. Aluminum panel

First, a double aluminum panel is considered which has been investigated by means of numerical simulations and experiments in [14]. The panel is made up from two 1220 mm × 2030 mm aluminum plates with thickness 1 and 2 mm separated by a 50.8 mm cavity filled with a fibrous material. The aluminum panels, with material properties given in table I, are linked with five C-section aluminum channels spaced by a distance of 508 mm. The channels are modeled as line connections with a translational stiffness $K_t' = 22.8 \cdot 10^6\,\mathrm{N/m^2}$ and a rotational stiffness $K_r' = 3.675 \cdot 10^3\,\mathrm{Nm/rad\,m}$ in the periodic model and WBM as suggested in [14]. The model of Davy only accounts for a mechanical compliance $C_t' = 1/K_t'$. Contrary to [14], the same value $K_t' = 22.8 \cdot 10^6\,\mathrm{N/m^2}$ is used in the model of Davy. The fibrous material in the cavity is modeled as an equivalent fluid. The adjusted wave number and damping of the fluid has been calculated with the Biot-Johnson-Allard model [29] using following material properties [14]: flow resistivity $\sigma = 17700\,\mathrm{Ns/m^4}$, tortuosity $\alpha_\infty = 1.0$, porosity $\phi = 0.91$, viscous characteristic length $\Lambda = 128\ \mu$m, and thermal characteristic length $\Lambda' = 376\ \mu$m.

3.2. Wooden floor

Second, a wooden floor is considered, consisting of 25 mm matched boards in floor and ceiling. The boards are coupled by wooden studs with height $h_{\mathrm{b}} = 220$ mm (equal to the cavity depth), width $w_{\mathrm{b}} = 67$ mm and spacing distance $d = 600$ mm. The cavity is filled with a fibrous material, which is modeled by means of the same equivalent fluid model as described in section 3.1. The wooden studs are modeled as either rigid line connections or beams. In the WBM, a floor with dimensions 3 m by 4 m is considered with seven 3 m long studs placed symmetrically around the middle of the floor. The material properties

used for the wooden studs and ceiling boards are given in table I. When modeling the wooden studs as separate beam elements, following mechanical properties are used: $I_x = w_\mathrm{b} h_\mathrm{b}^3/12 = 5.945 \cdot 10^{-5}\,\mathrm{m}^4$, $J_y = 0.2694 h_\mathrm{b} w_\mathrm{b}^3 = 1.783 \cdot 10^{-5}\,\mathrm{m}^4$, $I_w = 0$, $m'_\mathrm{b} = \rho_\mathrm{b} w_\mathrm{b} h_\mathrm{b} = 7.37\,\mathrm{kg/m}$, and $I'_\mathrm{bS} = \rho_\mathrm{b} w_\mathrm{b} h_\mathrm{b} \left(w_\mathrm{b}^2 + h_\mathrm{b}^2\right)/12 = 3.248 \cdot 10^{-2}\,\mathrm{kg\,m}$.

3.3. Plasterboard walls with steel stud frame

Third, a number of double gypsum plasterboard walls with width 3.25 m and height 2.95 m is considered. The first double gypsum plasterboard wall, denoted by 12.5/45/12.5 mm, has a cavity thickness of 45 mm and 12.5 mm thick leafs. The cavity is either empty or filled with a 40 mm mineral wool layer. The second wall, denoted by 3x12.5/100/3x12.5 mm, has a cavity thickness of 100 mm with three 12.5 mm thick gypsum plasterboards screwed on each side. The cavity is either empty or filled with a 75 mm mineral wool layer. The leafs are screwed to a steel stud frame consisting of a top and bottom railing and 7 vertical steel studs type CW. Two of the vertical studs are fixed to the concrete frame of the laboratory. A sealant is attached to the back of these studs to avoid leakage. The central 5 studs are placed symmetrically with a spacing of 60 cm. The distance between screws is 25 cm for the outer leafs. For the inner leafs of the second wall, the screw distance is 75 cm. The plasterboard plates have a nominal surface mass of $9\,\mathrm{kg/m^2}$. The material properties used in the simulations for the gypsum plasterboard leafs are given in table I. For the second double wall, the leafs of the double panels are modeled as one equivalent thin plate with thickness 37.5 mm, adjusting the Young's modulus to 278 MPa to account for the discrete coupling. The mineral wool is taken into account by modeling the air in the cavity as an equivalent fluid. It is thus implicitly assumed that the mineral wool fills the entire cavity. The model of Biot-Johnson-Allard [29] is used with following material properties: $\sigma = 10000\,\mathrm{Ns/m^4}$, $\alpha_\infty = 1.05$, $\phi = 0.98$, $\Lambda = 150\ \mu$m, and $\Lambda' = 300\ \mu$m. Numerical simulations have shown that this equivalent fluid model is a good approximation of a full Biot model for poro-elastic layers when no mechanical coupling exists between the absorbing layer and the plates [30]. For the walls with empty cavity, damping in the air layer is accounted for by using a frequency dependent absorption coefficient $\alpha_s(f)$ for the inner surfaces of the leafs [26]. The absorption is uniformly distributed over the air cavity (with volume V and depth d), by making the wave number in air complex according to equation (2). The equivalent reverberation time of the cavity $T_{eq}(f)$ is determined from

$$T_{eq}(f) = \frac{0.16V}{A_{eq}(f)} = \frac{0.16d}{2\alpha_s(f)} \tag{29}$$

with $A_{eq}(f)$ the equivalent absorption area of the cavity and

$$\alpha_s(f) = C_\alpha f^{0.41}. \tag{30}$$

The frequency dependency of the absorption coefficient is chosen such that the attenuation constant changes with frequency as given by the empirical model of Delany and Bazley [31] for the wave propagation in porous materials. The parameter C_α, which is related to the amount of viscous damping and the roughness of the surfaces, is taken equal to 0.0005 for the plasterboard walls with empty cavity [26].

3.4. Plasterboard wall with timber stud frame

Finally, a plasterboard wall with a timber stud frame is considered, which was used in an experimental study by Roozen *et al.* [28]. The wall (width 3.71 m, height 2.77 mm) consists of 12.5 mm gypsum fiberboards screwed on a timber frame with timber studs ($h_\mathrm{b} = 160$ mm, $w_\mathrm{b} = 80$ mm) and spacing distance $d = 600$ mm. The cavity with depth 160 mm is entirely filled with glass wool with density $12.5\,\mathrm{kg/m^3}$. To investigate the influence of panel fastening, the fiberboards were fastened with screws in different configurations changing the number of screws and the tightness of the screws. In this paper, only configurations 1 and 4 [28, Table 1] are considered with the minimum and maximum number of screw connections. In configuration 1, the plaster boards (three in total on each side) are only fixed in each corner by screws at the top and bottom, at a distance of 140 mm of the panels edge. In configuration 4, seven rows of screws are used to fix the panels to the studs. A detailed description of the test specimen and mounting configurations can be found in [28]. In the WBM, the timber frame studs are modeled as rigid line connections or as separate beam elements. The material properties used in the simulations for the wooden studs and gypsum fiberboard leafs are given in table I. The glass wool is modeled by means of the same equivalent fluid model as described in section 3.3, but reducing the flow resistivity to $\sigma = 5000\,\mathrm{Ns/m^4}$. Following mechanical properties are used for the beams: $I_x = 2.731 \cdot 10^{-5}\,\mathrm{m}^4$, $J_y = 0.229 h_\mathrm{b} w_\mathrm{b}^3 = 1.876 \cdot 10^{-5}\,\mathrm{m}^4$, $I_w = 0$, $m'_\mathrm{b} = 6.4\,\mathrm{kg/m}$, and $I'_\mathrm{bS} = 1.707 \cdot 10^{-2}\,\mathrm{kg\,m}$.

4. Numerical results and discussion

In this section, the test panels described in the previous section are used to numerically analyze the sound transmission through double walls with structural connections. First, results of the WBM are compared with infinite plate models. The structure-borne transmission path is compared separately to investigate differences between the models and analyze the validity of the decoupled approach. Afterwards, the difference between a simplified rigid stud model and a more detailed beam model is investigated. Finally, a parametric study shows the influence of stud distance, edge connections, and room dimensions on the TL.

4.1. Comparison with infinite plate models

The TL of the aluminum double panel is calculated with the decoupled approach of Davy [7], the periodic model of Legault and Atalla [14] and the WBM. While results

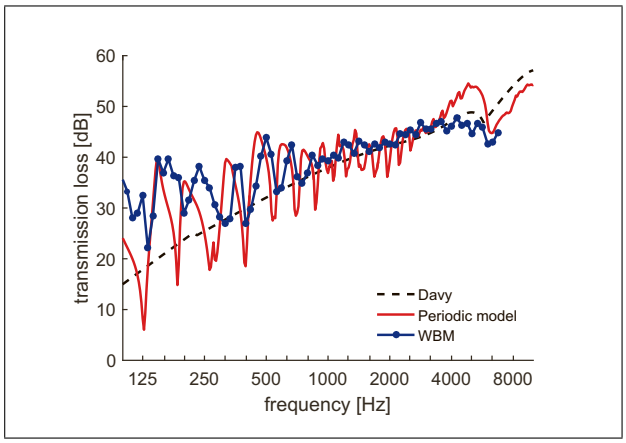

Figure 2. TL of the structure-borne transmission path through the studs of the aluminum double panel. Simulation results for the decoupled model of Davy [7], the infinite periodic plate model of Legault and Atalla [14], and the WBM in 1/12 octave bands.

are only shown for the double aluminum panel, a similar analysis has been performed for the wooden floor and the double plasterboard walls, from which the same general conclusions can be drawn.

First, the structure-borne transmission path through the structural connections is studied separately, thus not taking into account the airborne transmission path. For the decoupled approach of Davy, the calculation is straightforward as the structure-borne transmission coefficient is determined separately in the model. For the WBM, the plate equations (12) and (13) are adjusted by disregarding the effect of the cavity pressure $\underline{p}_{\mathrm{a}}^{(2)}$. Similar adjustments can be made to the infinite periodic plate model of [14]. For the infinite plate models, field incidence is assumed with angles of incidence ranging from 0° to 78°. In the WBM, following dimensions have been assumed for the source and receiving room: $L_x^{(1)} \times L_y^{(1)} \times L_z^{(1)} = 3.35\,\mathrm{m} \times 3.0\,\mathrm{m} \times 5.09\,\mathrm{m}$ and $L_x^{(3)} \times L_y^{(3)} \times L_z^{(3)} = 3.35\,\mathrm{m} \times 3.0\,\mathrm{m} \times 6.09\,\mathrm{m}$, with a horizontal offset of 0.25 m between the two rooms to reduce the modal coupling. The source is placed in the back corner of the source room and the TL is determined by measurement formula (28).

Figure 2 shows the TL of the structure-borne transmission path through the aluminum panel. The three models agree fairly well over the entire frequency range of interest. The decoupled approach of Davy disregards the periodic behaviour of the plate and therefore cannot predict the dips and peaks associated with the pass-and-stop bands of the structure. The dips around the pass bands are most pronounced in the periodic model results. The dips are still visible in the WBM results at low and mid frequencies, but the oscillations in the WBM results are negligible above 800 Hz. As stated by Craik and Smith [32], the TL features with well defined dips and peaks predicted for periodic structures is usually not observed for real structures, as they are not sufficiently well built that they can be considered periodic. These simulations indicate that the non-observation of the dips and peaks can furthermore be

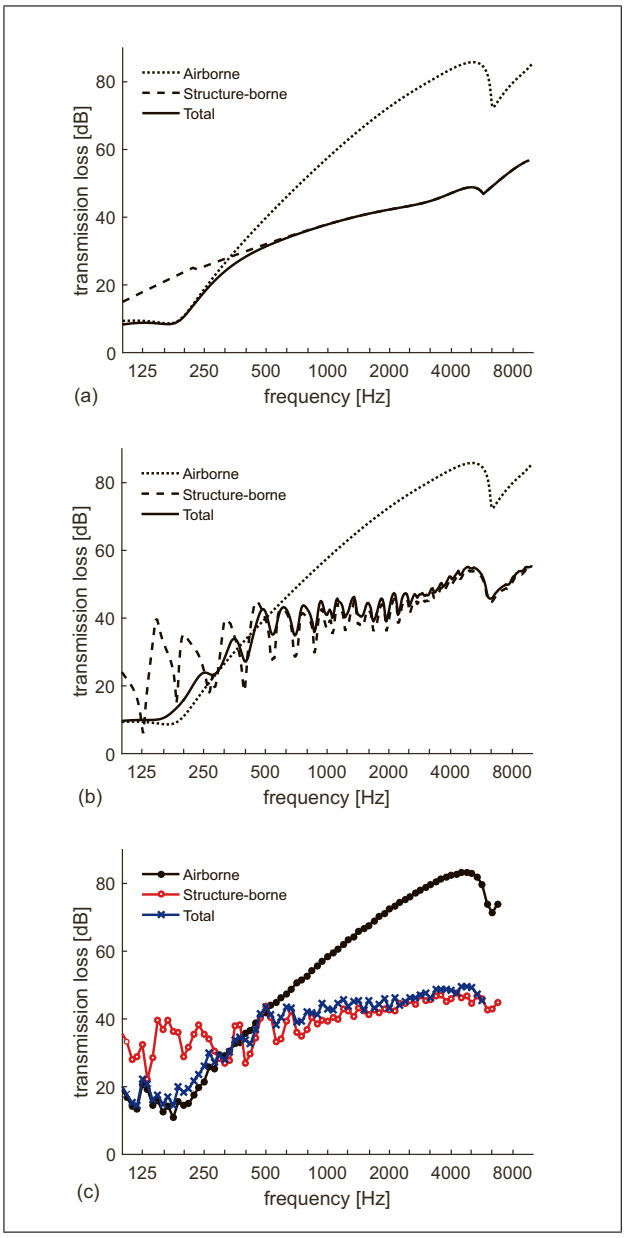

Figure 3. Airborne, structure-borne and total TL of the aluminum double panel. Simulation results for (a) the decoupled model of Davy [7], (b) the infinite periodic plate model of Legault and Atalla [14], and (c) the WBM in 1/12 octave bands.

related to the finite dimensions of real structures. Due to the limited amount of studs, the pass-and-stop band behaviour cannot fully develop. The dips and peaks will be smoothed by averaging the results in one-third octave bands. The decoupled approaches like the model of Davy, which are mainly of interest for predictions in one-third octave bands, will therefore also agree better with band-averaged TL values.

Figure 3 compares the total transmission loss of the aluminum double panel with the structure-borne transmission loss $\mathrm{TL_s}$ of Figure 2 for the two infinite plate models and the WBM. The TL of the aluminium panel without structural connections is also shown, representing the transmission loss $\mathrm{TL_a}$ of the airborne transmission path. For the

infinite plate models, TL_a has been calculated with the transfer matrix method (TMM) [29]. Below 400 Hz, the airborne transmission path is dominant. At higher frequencies the structure-borne transmission across the channels is more important. For the decoupled approach (Figure 3a), the total TL is always lower than both the airborne and structure-borne TL due to the inherent assumption of the model that $TL = -10\lg\left(10^{-TL_a/10} + 10^{-TL_s/10}\right)$. At the bridge frequency of 335 Hz where TL_a equals TL_s, the total TL is 3 dB lower than $TL_a = TL_s$. For the periodic model (Figure 3b) and the WBM (Figure 3c), the total TL is still determined by the dominant transmission path, but it can be higher than the airborne or structure-borne TL. This shows that there is an interaction between the airborne and structure-borne transmission path which is neglected in the decoupled approach. At low frequencies, the structural connections can improve the TL of the double wall without connections due to an increased stiffness. This is in agreement with the experimental observation of Hongisto *et al.* [1]. Similarly, at higher frequencies the air in the cavity can slightly restrict the movement of the panels, thus reducing the vibrations of the second panel transmitted by the structural connections.

The main restriction of the WBM is that it is computationally more expensive than the infinite plate models, especially when a large number of room and plate modes have to be taken into account, i.e. for structures with low stiffness and at higher frequencies. Table II gives an idea of the relative computation times for the three models on a standard pc to calculate the TL of different structures considered in the paper. While the WBM calculation time increases significantly at higher frequencies, the WBM is computationally very efficient at low frequencies. Furthermore, the WBM is computationally more efficient compared to classical numerical methods like the finite element method [33] and thus more suitable to investigate the influence of geometric parameters like room and plate dimensions or stud location in a broader frequency range.

4.2. Rigid line connections versus beams

Here, the wooden floor of section 3.2 is considered. The TL of the wooden floor is calculated with the periodic model of Legault *et al.* [14] and the WBM. In the WBM, the wooden floor is placed between two rooms with width 3 m and length 4 m. The source and receiving room have a height of 6.09 m and 5.12 m, respectively. Figure 4 shows the predicted TL when the wooden studs are either modeled as rigid line connections or as separate beam elements. As a reference, the TL of the wooden floor without structural connections is also shown. The mass-spring-mass resonance dip is visible around 40 Hz for the floor without studs. The coincidence dip of the wooden boards is observed around 630–800 Hz. The wooden studs influence the TL in the entire frequency range of interest. The structure-borne sound transmission is dominant above 63 Hz. Below 63 Hz, the studs improve the TL thanks to the increased stiffness. Above the coincidence dip, the general trends are the same for the periodic model and the

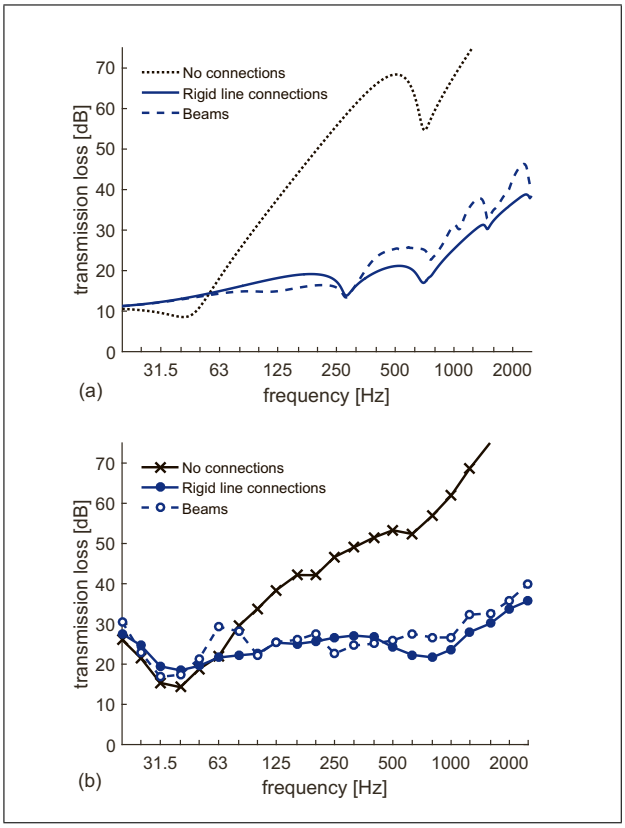

Figure 4. (a) Infinite periodic plate simulations and (b) WBM simulations in 1/3 octave bands of the TL of the wooden floor without and with wooden studs modelled as rigid line connections or beams.

WBM. At lower frequencies, the WBM results are on average $5 - 10$ dB higher than the infinite plate results due to the diffraction effect at the edges of the structure. The periodic model predicts two additional dips at 280 Hz and 1500 Hz linked to structural resonances and pass bands of the periodic structure. This pass- and stop-band behaviour is not seen for the finite plate with seven rigid studs. Below 100 Hz, the WBM fluctuations reflect the modal behaviour of the finite structure and the rooms. When comparing the rigid line models with the beam models, slight differences can be observed. Above 250 Hz (for the periodic plate model) and 500 Hz (for the WBM), the TL is approximately 3 dB larger for the beam model in most frequency bands thanks to the additional mass of the wooden studs. The periodic model predicts a slightly lower TL for the beam model between 50 Hz and 250 Hz. At very low frequencies, no differences are seen in the periodic model results. The beams can however influence the modal behaviour of the double wall which determines the TL at low frequencies. As a result, larger differences are observed between the two WBM models below 100 Hz.

4.3. Influence of stud spacing

Figure 5 shows the influence of the spacing between the wooden studs on the TL of the wooden floor. Three different stud spacings are considered: 0.6 m (the reference value), 0.9 m and 1.2 m. The studs are modeled as rigid

Table II. Computation times for the decoupled model of Davy [7], the infinite periodic plate model of Legault and Atalla [14], and the WBM to calculate the TL at 100 Hz, 500 Hz and 1000 Hz of different structures on a HP notebook with Intel(R) Core(TM) i7-6500U 2.50 GHz processor.

	Decoupled model			Periodic model			WBM		
	100 Hz	500 Hz	1000 Hz	100 Hz	500 Hz	1000 Hz	100 Hz	500 Hz	1000 Hz
Aluminum panel	0.19 s	0.048 s	0.022 s	0.73 s	1.1 s	2.9 s	0.10 s	11 s	74 s
Wooden floor (rigid)	0.12 s	0.030 s	0.051 s	0.41 s	4.1 s	11 s	0.032 s	0.19 s	3.7 s
Wooden floor (beam)	–	–	–	3.5 s	16 s	18 s	0.073 s	0.35 s	5.2 s
Plasterboard wall 12.5/45/12.5 mm	0.31 s	0.065 s	0.041 s	4.1 s	0.66 s	0.52 s	0.056 s	6.0 s	46 s

line connections. In the WBM model, the floor (length 3 m and width 4 m) has seven, five and four wooden studs, respectively. For each test case, the 3 m long studs are symmetrically placed around the middle of the floor.

In the model of Davy (Figure 5a), the stud spacing determines the amount of line couplings per area and thus the amount of structure-borne sound transmission. The larger the spacing between the studs, the larger the structure-borne TL which dominates above 40 Hz. This behaviour is not observed in the periodic plate (Figure 5b) and WBM (Figure 5c) results. In the periodic model (Figure 5b), the stud spacing has little effect on the TL at and above the coincidence dip around 630–800 Hz. At mid frequencies, the TL changes drastically as the stud distance determines the pass- and stop-bands of the periodic floor. The mass-spring-mass resonance frequency of the wooden floor without studs around 40 Hz increases to approximately 80 Hz, 125 Hz, and 260 Hz for the stud spacing of 1.2 m, 0.9 m, and 0.6 m respectively. The studs act as an added stiffness in parallel with the stiffness of the air in the cavity. As a result, the mass-spring-mass resonance frequency of the double panel increases [12, 34].

The WBM results (Figure 5c) follow the general trends of the periodic model. The TL is almost independent of the stud spacing above 500 Hz. At mid frequencies, dips can be observed in the TL for the cases $d = 90$ cm and $d = 120$ cm at similar frequencies like the periodic plate results, although the resonances are less pronounced. The results of the periodic model and the WBM confirm the findings of the experimental study of Hongisto *et al.* [1]. The effect of the spacing of wooden studs was the largest at low and mid frequencies where a shift in resonance dips was seen. At higher frequencies, the influence was very small with only a slight increase in TL with increasing stud distance.

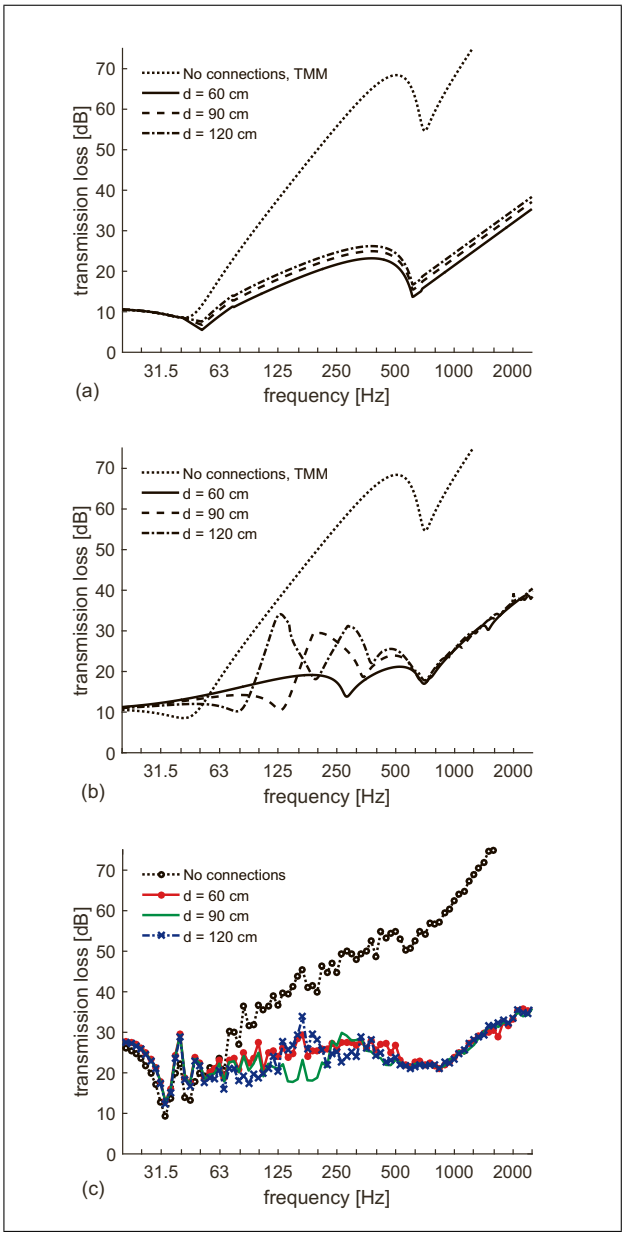

Figure 5. Influence of stud spacing on the TL of the wooden floor. Simulation results for (a) the decoupled model of Davy [7], (b) the infinite periodic plate model of Legault and Atalla [14], and (c) the WBM in 1/12 octave bands.

4.4. Influence of edge connections

When mounting lightweight double walls, studs are usually placed at the vertical edges of the wall. Similarly, top and bottom railings are needed, especially in the case of a steel stud frame. The additional vibration transmission through the peripheral studs can be larger than transmission through central studs due to the higher plate mobility at the edges [35]. Secondly, the peripheral studs and railings are usually connected to the laboratory frame. As

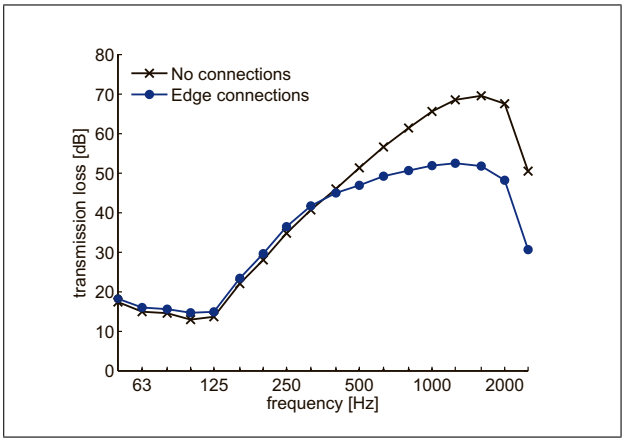

Figure 6. TL of the double gypsum fiberboard wall 12.5/45/12.5 mm with cavity absorption. WBM simulations in 1/3 octave bands without structural connections and with edge connections.

a result, the vibrations can be transmitted between the wall leaves via the frame of the laboratory test opening. While the first effect is only important for double walls mounted on a single frame, the structural transmission path around the edges through the laboratory frame will also be important for double lightweight walls mounted on double frames. The results of an inter-laboratory test for lightweight walls [36] indicate that structural coupling around the perimeter can significantly alter the TL over the majority of the building acoustics frequency range. The amount of coupling strongly depended on the type of lining material used around the perimeter of the aperture. The simulation results in Figure 6 confirm the important influence of edge connections on the TL of lightweight walls. The TL of the double gypsum fiberboard wall 12.5/45/12.5 mm with cavity absorption has been simulated with the WBM. In the first model, no structural connections are taken into account. The second model incorporates edge connections around the perimeter of the wall with dimensions 3.25 m × 2.95 m. The edge connections are modeled as rotational spring with zero compliance, meaning that the rotation of the two panels will be the same at the edges and vibrations can be transmitted by bending moments. The edge connections clearly reduce the TL from 400 Hz upwards.

4.5. Influence of room dimensions

The room dimensions will influence the measured TL, especially below the Schroeder frequency of the rooms. For single walls with a low modal density and for double walls, the variance caused by different room dimensions may be important even above the Schroeder frequency of the rooms [27]. In this section, the influence of the source room dimensions on the TL of the double plasterboard wall 3x12.5/205/3x12.5 mm with or without cavity absorption is investigated. In the models, the central studs are either neglected, thus only taking into account the airborne transmission path, or modeled as line connections

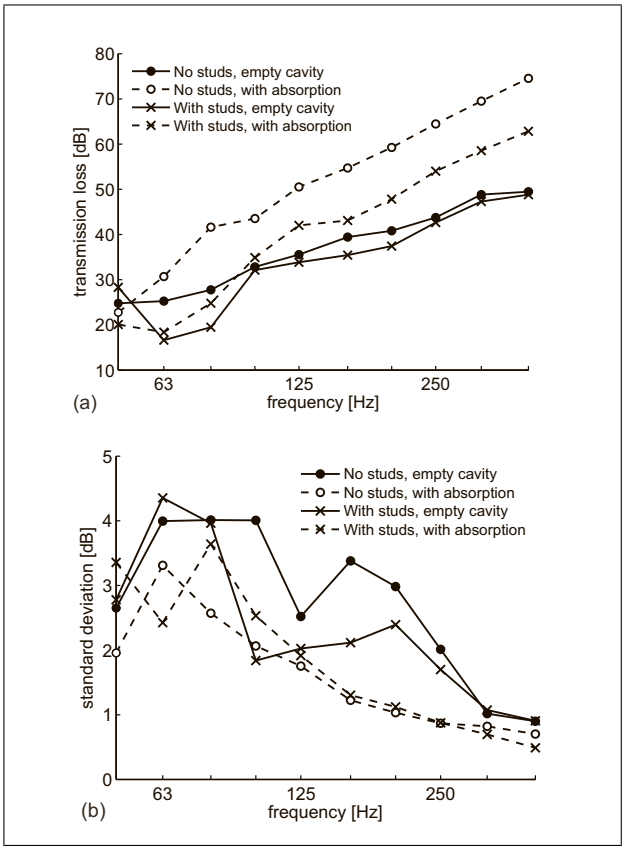

Figure 7. Influence of source room dimensions on the TL of four double gypsum fiberboard walls 3x12.5/205/3x12.5 mm. (a) Mean value and (b) standard deviation for 50 different source rooms with volume > 50 m^3. WBM simulations in 1/3 octave bands.

with a frequency dependent, equivalent translational stiffness $K'_t(f)$ according to [8, 20, 21],

$$\lg K'_t = 0.6286x^3 - 4.4051x^2 + 10.3323x - 2.0722 \quad (31)$$

with $x = \lg f$, and no rotational stiffness ($K'_r = 0$). Edge connections are disregarded in all the models. The effect of the source room dimensions is analysed by means of Monte Carlo simulations. The TL is calculated for 50 different source rooms. While varying the dimensions of the source room, the dimensions of the receiving room (width 4.0 m, height 3.4 m, length 5.25 m) and the plate dimensions (3.25 m × 2.95 m) are fixed. In each case, the transmission coefficient is averaged for 5 randomly chosen source positions at a distance of minimum 0.7 m from the room boundaries and the other source positions. All rooms have a volume of at least 50 m^3 and a frequency independent value of 1.5 s is used for the reverberation time so that the requirements of the standard ISO 10140 [25] for laboratory TL measurements are met.

Figure 7 shows the mean value and standard deviation of the ensemble for the four different double plasterboard walls. Generally, the TL is the highest for the wall without studs and with cavity absorption (Figure 7a). The lowest TL is predicted for the wall with studs and without cavity absorption which agrees with measurement results [1] and

results from classical models [2, 5, 6] found in literature. In the case of an empty cavity, the influence of the studs is however small as the airborne transmission path is still important at lower frequencies. When placing absorption in the cavity, the airborne path is diminished and the influence of the studs is larger. The cavity absorption improves the TL of the double wall without studs by $15 - 20$ dB, while the TL of the double wall with studs only increases by $5 - 10$ dB. Figure 7b shows that the variability with room dimensions generally decreases with frequency as expected. The standard deviation is the largest for the double walls without cavity absorption, with values around 4 dB below 100 Hz. At higher frequencies, the variability is still significant and the largest values are found for the double wall with empty cavity and without studs. Including studs or cavity absorption decreases the influence of the room dimensions on the TL.

These results illustrate the theoretical variation in TL that can be expected by changing the source room dimensions, under the assumption that the measurement error related to spatial sampling of the sound field is zero. In measurements, the true average sound pressure levels in the rooms are not known. Estimations based on a limited number of microphone positions generally increase the uncertainty. The reproducibility uncertainty related to geometrical parameters like room dimensions is however much larger than the repeatability uncertainty related to microphone positions, especially for the case of lightweight double walls [27].

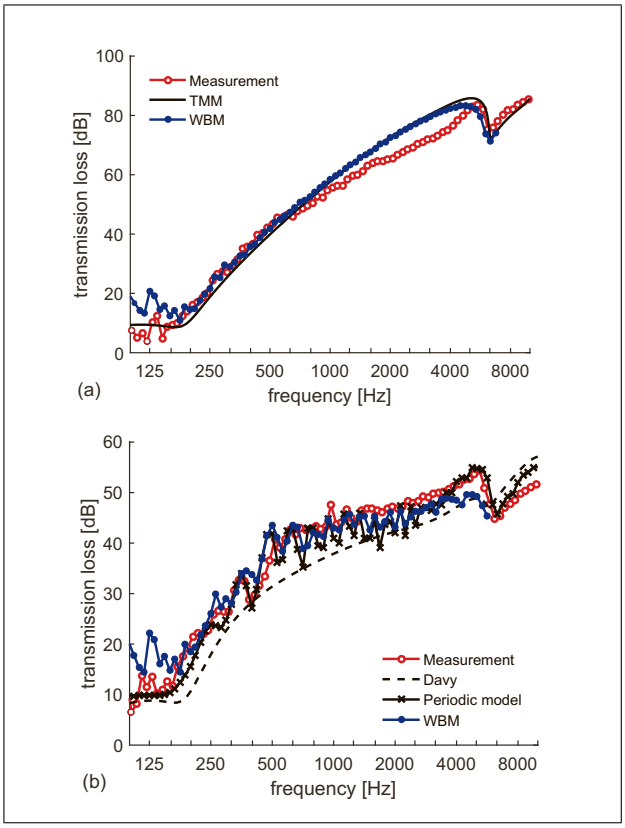

Figure 8. Measured and simulated TL (taken from [14]) of the aluminum double panel (a) without channels and (b) with 5 C-section channels.

5. Experimental validation

5.1. Aluminum double panel

A first validation example considers the double aluminum panel described in section 3.1. The TL of the same double aluminum panel without channels was also measured in [14]. Figure 8a shows the measured 1/12 octave band TL for the panel without channels, together with TMM and WBM predictions. For the TMM, field incidence is assumed with angles of incidence ranging from 0° to 78°. The setup of the WBM has been described in section 4.1. The TMM results agree reasonably well with the measured TL. Between 1000 Hz and 5000 Hz, the TL is slightly overestimated, which is possibly related to structural flanking transmission around the edges of the panel in the measurement setup. The WBM results converge to the TMM results above 500 Hz. The overestimation of the WBM below 200 Hz can be attributed to the fact that no detailed information was available on the measurement setup and transmission rooms. The room dimensions have been randomly chosen. Furthermore, it is assumed that the TL is measured according to the pressure method of ISO 10140 [24], which leads to higher TL values compared to the intensity method of ISO 15186 [37] at low frequencies [27]. Between 200 Hz and 500 Hz, the WBM predicts slightly higher TL values than the TMM and agrees better with measurement results. The coincidence dip around 6300 Hz is well predicted by both models.

For the aluminum panel with channels (Figure 8b), the decoupled model of Davy underestimates the TL below the coincidence dip. This may be partly explained by an underestimation of the actual plate damping or the fact that the mass of the channels is neglected. The periodic model gives reasonable agreement in most of the frequency range considered. While there is a good agreement between measurement and periodic model results around the first pass band dip at 400 Hz, the dips predicted at higher frequencies are not observed in the measurement results. As a result, the model slightly underestimates the TL between 500 Hz and 3000 Hz, where the TL is dominated by structure-borne sound transmission across the channels. Increasing the plate damping or including the mass of the channels would increase the predicted TL. At higher frequencies, there is a good agreement and the coincidence dip at 6300 Hz is well predicted. The WBM results correspond well with the measured TL in a broad frequency range with only an underestimation around 4000 Hz. Again, the pass- and stop-band behaviour predicted with the periodic model is not observed as clearly in the WBM results. Below 200 Hz, the WBM overestimates the TL like for the panel without channels. At high frequencies, the WBM results converge to the results of the decoupled model of Davy.

5.2. Plasterboard walls with steel stud frame

Secondly, the double gypsum plasterboard walls described in section 3.3 are considered. The TL was measured in the large transmission opening of the reverberation chambers of the Laboratory of Acoustics at KU Leuven with the pressure method according to ISO 10140 [24]. The transmission opening has a width of 3.25 m and a height of 2.95 m.

The TL of the different double gypsum fiberboard walls is simulated with the WBM (Figure 9). Details of the reverberation chambers and the geometry of the wave based model can be found in [26]. Four different models have been set up:

1. a reference model without structural connections;
2. a model where the 5 central steel studs are modeled as rigid line connections and edge connections are disregarded;
3. a model where the 5 central steel studs are modeled as spring line connections and edge connections are disregarded;
4. a model where the 5 central steel studs are modeled as spring line connections and rigid edge connections are incorporated.

For the spring line connections in model 3 and 4, a frequency dependent, equivalent translational stiffness $K'_t(f)$ according to equation (31), and no rotational stiffness ($K'_r = 0$) is used. The connections at the four edges in model 4 are modeled as a rotational spring with zero compliance ($C'_r = 0$).

For the wall 12.5/45/12.5 mm without cavity absorption (Figure 9a), the WBM without structural connections already gives good agreement in most of the frequency range. This indicates that the airborne transmission path is dominant for this wall. Indeed, the influence of the structural connections is limited in the WBM results, although the rigid line connections give an underestimation of the TL at high frequencies. Furthermore, the TL predictions increase around the mass-spring-mass resonance dip at 125–160 Hz when taking into account structural connections and better agreement is achieved with measurement results. Again, this confirms that structural connections can improve the TL below and around the mass-spring-mass resonance frequency due to the increased stiffness of the double wall.

When the cavity is filled with mineral wool (Figure 9b), the airborne transmission path is reduced and the structure-borne transmission path is more important. Below the mass-spring-mass resonance frequency, the TL is again underestimated by the WBM without structural connections, while the other models with structural connections give better agreement. The WBM without structural connections agrees well with the measurement results between 125 Hz and 250 Hz, indicating that the airborne transmission is dominant. In this frequency range, the structural connections do not influence the sound transmission significantly, although the WBM with spring line connections underestimates the TL. Structure-borne transmission across the studs is important from 250 Hz upwards.

For the double walls 3x12.5/100/3x12.5 mm with empty cavity (Figure 9c) and with cavity absorption (Figure 9d), the mass-spring-mass resonance frequency is significantly lower. As a result, the structure-borne sound transmission is dominant in the entire frequency range of interest, even for the double wall with empty cavity. In the frequency range where structure-borne sound transmission dominates, i.e. 315−5000 Hz for the wall 12.5/45/12.5 mm with cavity absorption and 50–5000 Hz for the walls 3x12.5/100/3x12.5 mm, the TL is strongly influenced by the type of structural coupling. When the studs are modeled as rigid line connections, the structure-borne sound transmission is overestimated and the overall TL is underestimated. The equivalent translational spring model overestimates the TL at higher frequencies. Generally, the model with spring line connections and edge connections agrees best with the measurement results. These results indicate that vibration transmission around the edges through the concrete frame of the laboratory were important at mid and high frequencies for these double walls with high direct sound insulation. It can be noted that the assumption of a perfect line connection can be questioned, especially at higher frequencies, knowing that the panels are only fixed at discrete positions to the studs [4, 38]. In general, the structure-borne sound transmission can be influenced by small details, as observed in experiments [1, 28] and round robin tests [39]. The loss factor of the plates, which was estimated in the model, may also influence the TL significantly [17].

5.3. Plasterboard wall with timber stud frame

Finally, the timber stud wall described in section 3.4 is considered. The TL was measured in the test facility at TGM, Vienna [28], according to ISO 10140 [24]. The source and receiving room have a depth of respectively 5.24 m and 5.90 m and a height of respectively 2.81 m and 2.82 m. The width of the rooms is equal to the width of the wall (3.71 m). Figure 10 shows the measured TL for two configurations of panel fastening (i.e. configuration 1 and 4 of [28, table 1]), revealing that the arrangement of the screws has a considerable influence. The TL of the two configurations with the minimum and maximum number of screws differs up to 15 dB.

Four WBM models have been set up to simulate the TL:

1. a reference model without structural connections;
2. a model where the timber studs are modeled as rigid line connections;
3. a model where the timber studs are modeled as beam elements;
4. a model where the timber studs are disregarded and 8 rigid point connections are incorporated at the position of the screws of configuration 1.

In total, nine studs are incorporated in model 2 and 3: seven vertical studs with spacing distance 625 mm (including the studs at the vertical edges), and two horizontal studs at the top and bottom. The fourth case is included as an alternative model of configuration 1, as it is expected

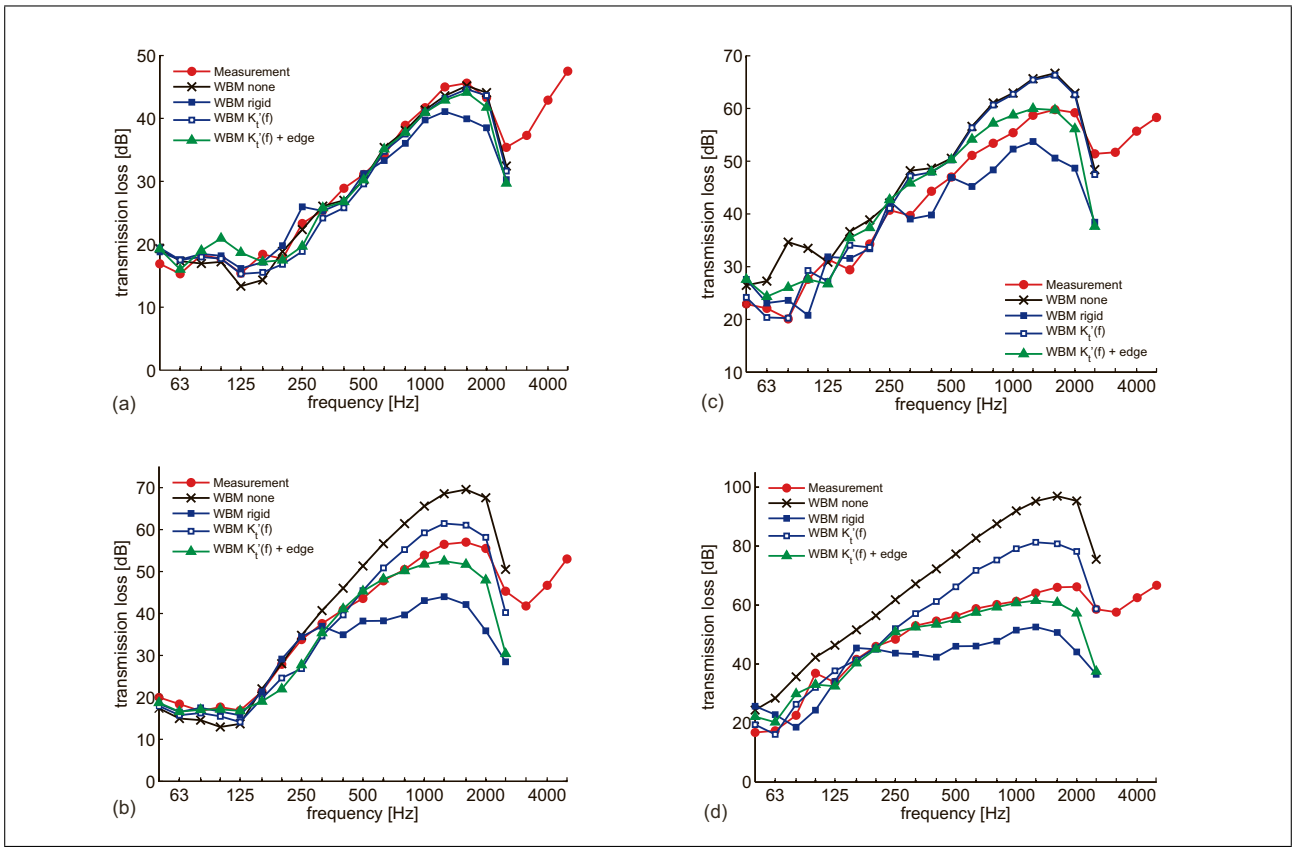

Figure 9. WBM simulations and experimental results in 1/3 octave bands of the TL of double gypsum fiberboard walls with steel studs. (a) 12.5/45/12.5 mm without cavity absorption, (b) 12.5/45/12.5 mm with cavity absorption, (c) 3x12.5/100/3x12.5 mm without cavity absorption, and (d) 3x12.5/100/3x12.5 mm with cavity absorption.

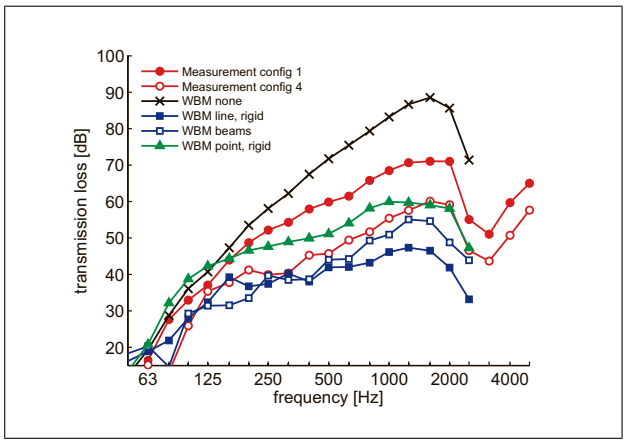

Figure 10. Measured TL (taken from [28]) and WBM simulations in 1/3 octave bands of the plasterboard wall with timber stud frame. Configuration 1 with screws at bottom and top only and configuration 4 with 7 rows of screws firmly fixed.

that the assumption of a perfect line coupling between the studs and the plates may not be valid [4, 35].

The reference model without structural connections overestimates the TL in the entire frequency range of interest, indicating the important influence of the timber stud frame. Even when the plaster boards are only fixed in the corners (configuration 1), the structural connections cannot be neglected, especially at higher frequencies. This is also illustrated by the significant decrease in the predicted TL when 8 rigid point connections are included in the WBM. The WBM with rigid line connections agrees reasonably well with the measured TL of configuration 4 up till 315 Hz, but clearly underestimates the TL at higher frequencies. There is a better agreement above 500 Hz when the timber studs are modeled as separate beam elements, although the TL is still underestimated by 5 dB on average. The WBM disregards the discrete screw connections between the panels and the studs. The measurement results of Roozen *et al.* [28] clearly show that small details like screw connections and panel fastening can influence the structure-borne sound transmission, especially at higher frequencies. It is therefore difficult to accurately predict the TL in this frequency range as these details are not incorporated in the current model. While the assumption of line connections can give reasonable results in some cases, more detailed models should be developed, including for example rigid or spring point connections between plates and beams.

6. Conclusions

In this paper, the wave based methodology has been extended for the investigation of the sound transmission

through double walls with structural connections. The deterministic model accounts for the modal behaviour of the rooms and the structure. Comparison between WBM results and infinite plate results show that the finite dimensions of the walls can have a significant influence on the sound insulation, both at low frequencies and at higher frequencies. The pass- and stop-band behaviour observed for infinite periodic structures cannot fully develop in finite double walls. Below 250 Hz, the modal behaviour of the rooms will also play a role. The variability with room dimensions is the largest for double walls without cavity absorption. At and below the mass-spring-mass resonance frequency, the TL is improved thanks to the stiffness provided by the studs. For double walls with cavity absorption, the structure-borne transmission is dominant above a certain bridge frequency, which is determined by the specific configuration of the double wall and the structural connections. In this frequency range, the TL is influenced by the type of structural coupling (point or line connections, rigid, spring or beam connections), making accurate predictions difficult in building acoustical applications. Structure-borne sound transmission around the perimeter of the walls may also be important at mid and high frequencies. The stud spacing can influence the resonant behaviour of the TL at low and mid frequencies, but has limited effect at higher frequencies.

Acknowledgements

Arne Dijckmans was supported by a postdoctoral fellowship of the Research Foundation Flanders (FWO). Part of this research was performed within a research stay at the Acoustics Research Unit (Liverpool), funded by the FWO. The financial support is gratefully acknowledged.

References

[1] V. Hongisto, M. Lindgren, R. Helenius: Sound insulation of double walls – An experimental parametric study. Acta Acust. united Ac. **88** (2002) 904–923.

[2] R. J. M. Craik: Sound Transmission through Buildings using Statistical Energy Analysis. Gower, England, 1996.

[3] R. J. M. Craik, R. Wilson: Sound transmission through masonry cavity walls. J. Sound Vib. **179** (1995) 79–96.

[4] R. J. M. Craik, R. S. Smith: Sound transmission through lightweight parallel plates. Part II: structure-borne sound. Appl. Acoust. **61** (2000) 247–269.

[5] B. Sharp: Prediction methods for the sound transmission of building elements. Noise Control Eng. J. **11** (1978) 53–63.

[6] F. J. Fahy, P. Gardonio: Sound and structural vibration, 2nd edition: Radiation, transmission and response. Academic Press, 2007.

[7] J. Davy: Sound transmission of cavity walls due to structure borne transmission via point and line connections. J. Acoust. Soc. Am. **132** (2012) 814–821.

[8] T. Vigran: Sound transmission in multilayered structures – Introducing finite structural connections in the transfer matrix method. Appl. Acoust. **71** (2010) 39–44.

[9] T. Vigran: Sound insulation of double-leaf walls – Allowing for studs of finite stiffness in a transfer matrix scheme. Appl. Acoust. **71** (2010) 616–621.

[10] G.-F. Lin, J. Garrelick: Sound transmission through periodically framed parallel plates. J. Acoust. Soc. Am. **61** (1977) 1014–1018.

[11] J. Brunskog, P. Hammer: Prediction model for the impact sound level of lightweight floors. Acta Acust. united Ac. **89** (2003) 309–322.

[12] M.S. Mosharrof, J. Brunskog, F. Ljunggren, A. Ågren: An improved prediction model for the impact sound level of lightweight floors: Introducing decoupled floor-ceiling and beam-plate moment. Acta Acust. united Ac. **97** (2011) 254–265.

[13] J. Wang, T. J. Lu, J. Woodhouse, R. S. Langley, J. Evans: Sound transmission through lightweight double-leaf partitions: theoretical modelling. J. Sound Vib. **286** (2005) 817–847.

[14] J. Legault, N. Atalla: Numerical and experimental investigation of the effect of structural links on the sound transmission of a lightweight double panel structure. J. Sound Vib. **324** (2009) 712–732.

[15] J. Legault, N. Atalla: Sound transmission through a double panel structure periodically coupled with vibration insulators. J. Sound Vib. **329** (2010) 3082–3100.

[16] F. X. Xin, T. J. Lu: Transmission loss of orthogonally rib-stiffened double-panel structures with cavity absorption. J. Acoust. Soc. Am. **129** (2011) 1919–1934.

[17] A. Dijckmans, G. Vermeir, W. Lauriks: Sound transmission through finite lightweight multilayered structures with thin air layers. J. Acoust. Soc. Am. **128**(2010) 3513–3524.

[18] C. Díaz-Cereceda, J. Hetherington, J. Poblet-Puig, A. Rodríguez-Ferran: A determinisctic model of impact noise transmission through structural connections based on modal analysis. J. Sound Vib. **330**) (2011) 2801–2817.

[19] A. Arjunan, C. J. Wang, K. Yahiaoui, D. J. Mynors, T. Morgan, V. B. Nguyen, M. English: Development of a 3D finite element acoustic model to predict the sound reduction index of stud based double-leaf walls. J. Sound Vib. **333** (2014) 6140–6155.

[20] J. Poblet-Puig, A. Rodríguez-Ferran, C. Guigou-Carter, M. Villot: The role of studs in the sound transmission of double walls. Acta Acust. united Ac. **95** (2009) 555–567.

[21] J. Davy, C. Guigou-Carter, M. Villot: An empirical model for the equivalent translational compliance of steel studs. J. Acoust. Soc. Am. **131** (2012) 4615–4624.

[22] L. Galbrun: Vibration transmission through plate/beam structures typical of lightweight buildings: Applicability and limitations of fundamental theories. Appl. Acoust. **71** (2010) 587–596.

[23] J. Brunskog: The influence of finite cavities on the sound insulation of double-plate structures. J. Acoust. Soc. Am. **117** (2005) 3727–3739.

[24] ISO-10140-2: Acoustics — Laboratory measurement of sound insulation of building elements – Part 2: Measurement of airborne sound insulation. 2010.

[25] ISO-10140-5: Acoustics — Laboratory measurement of sound insulation of building elements – Part 5: Requirements for test facilities and equipment. 2010.

[26] A. Dijckmans: Wave based calculation methods for sound-structure interaction. Application to sound insulation and sound radiation of composite walls and floors. Ph.D. thesis, Katholieke Universiteit Leuven, Department of Civil Engineering, 2011.

[27] A. Dijckmans, G. Vermeir: Numerical investigation of the repeatability and reproducibility of laboratory sound insulation measurements. Acta Acust. united Ac. **99** (2013) 421–432.

[28] N. B. Roozen, H. Muellner, L. Labelle, M. Rychtárikova, C. Glorieux: Influence of panel fastening on the acoustic performance of light-weight building elements: Study by sound transmission and laser scanning vibrometry. J. Sound Vib. **346** (2015) 100–116.

[29] J. F. Allard, N. Atalla: Propagation of Sound in Porous Media. Modelling Sound Absorbing Materials. 2nd Edition. John Wiley & Sons, Ltd, Chichester, 2009.

[30] A. Dijckmans: The influence of finite dimensions on the sound insulation of double walls. Proceedings of 7th Forum Acustium, Kraków, Poland, 2014, 1–6.

[31] M. A. Delany, E. N. Bazley, Acoustical properties of fibrous materials. Appl. Acoust. **3** (1970), 105–116.

[32] R. J. M. Craik, R. S. Smith: Sound transmission through double leaf lightweight partitions. Part I: Airborne sound. Appl. Acoust. **61** (2000) 223–245.

[33] B. Van Genechten, O. Atak, B. Bergen, E. Deckers, S. Jonckheere, J. Lee, A. Maressa, K. Vergote, B. Pluymers, D. Vandepitte, W. Desmet: An efficient wave based method for solving Helmholtz problems in three-dimensional bounded domains. Engineering Analysis with Boundary Elements **36** (2012) 63–75.

[34] J. S. Bradley, J. A. Birta: A simple model of the sound insulation of gypsum board on resilient supports. Noise Control Eng. J. **49** (2001) 216–223.

[35] C. Guigou-Carter, M. Villot: Analytical and experimental study of single frame double wall. Proceedings of the 6th European conference on noise control (Euronoise). Tampere, Finland, 2006, 1–6.

[36] R. S. Smith, P. Fausti, R. Pompoli: An investigation into the reproducibility values of the European inter-laboratory test for lightweight walls. Building Acoustics **6** (1999) 187–210.

[37] ISO-15186-1: Acoustics – Measurement of sound insulation in buildings and of building elements using sound intensity – Part 1: Laboratory measurements. 2000.

[38] C. Guigou-Carter, S. Bailhache, R. Foret, A. Igeleke: Characterization of metallic studs used in gypsum board single frame walls. Proceedings of the 9th European Conference on Noise Control (Euronoise). Prague, Czech Republic, 2012, 713–718.

[39] P. Fausti, R. Pompoli, R. S. Smith: An intercomparison of laboratory measurements of airborne sound insulation of lightweight plasterboard walls. Building Acoustics **6** (1999) 127–140.